DOI: ((insert here when preparing revised/final version))
Article type: (Full Paper)

Atmospheric pressure roll-to-roll plasma enhanced CVD of high quality silica-like bilayer encapsulation films

Fiona M. Elam,* Sergey A. Starostin, Anna S. Meshkova, Bernadette C. A. M. van der Velden-Schuermans, Jan B. Bouwstra, Mauritius C. M. van de Sanden, Hindrik W. de Vries.

_____

F. M. Elam, Dr. S. A. Starostin, B. C. A. M. van der Velden-Schuermans, Dr. J. B. Bouwstra
FUJIFILM Manufacturing Europe B.V.
P.O. Box 90156, 5000 LJ Tilburg
The Netherlands
Email: fiona_elam@fujifilm.eu

F. M. Elam, A. S. Meshkova, Prof. M. C. M. van de Sanden
Plasma and Materials Processing Group
Department of Applied Physics
Eindhoven University of Technology
P.O. Box 513, 5600 MB Eindhoven
The Netherlands

A. S. Meshkova, Prof. M. C. M. van de Sanden, Dr. H. W. de Vries
FOM Institute DIFFER – Dutch Institute For Fundamental Energy Research
P.O. Box 6336, 5600 HH Eindhoven
The Netherlands

_____

Abstract

A glow like atmospheric pressure dielectric barrier discharge in a roll-to-roll setup was used to synthesise 90 nm silica-like bilayer encapsulation films composed of a 30 nm dense 'barrier layer' and a comparatively less dense 60 nm 'buffer layer' onto a polyethylene 2,6 naphthalate substrate by means of plasma enhanced chemical vapour deposition. Tetraethyl orthosilicate was used as the precursor gas, together with a mixture of nitrogen, oxygen and argon. The microstructure, chemical composition, morphology and permeation properties of the films were studied as a function of the specific energy delivered per precursor molecule, and oxygen concentration in the gas mixture, during the deposition of the barrier layer. The presence of the buffer layer within the bilayer architecture critically enhanced the encapsulation performance of the bilayer films, and this in conjunction with increasing the specific energy delivered per precursor molecule during the barrier layer deposition to a value of 20 keV, enabled an effective water vapour transmission rate as low as 6.9×10^{-4} g m^{-2} day^{-1} (at 40 °C, 90% relative humidity) to be achieved. Furthermore, the bilayer film structure has given rise to a remarkable 50% reduction in deposition energy consumption per barrier area with respect to single layer silica-like films of equivalent encapsulation performance and thickness.

Introduction

Flexible electronics are an innovative array of devices that have the potential to revolutionise the electronic and energy markets. They cover a wide range of applications, from light-emitting or photovoltaic diodes to thin film transistors and solar cells. However, due to their particular chemical nature, exposure to environmental moisture and oxygen,[1–9] can result in oxidation and crystallisation of the main components.[4] Therefore, a suitable flexible thin film encapsulation barrier is required in order to extend device lifetime and ensure their commercial viability.

Aside from excellent moisture barrier performance and flexibility, these encapsulation foils must fulfil a specific set of requirements. They should be thermal and scratch resistant, smooth, durable and both simple and inexpensive to manufacture.[5] Thus far, these barrier coatings have typically consisted of single or multilayer stacks of silicon nitride (Si_3N_4), alumina (Al_2O_3), silica (SiO_2) or titania (TiO_2) layers deposited onto a flexible plastic substrate via various deposition methods.[2,4–24]

One such method is atmospheric pressure-plasma enhanced chemical vapour deposition (AP-PECVD). This pioneering technology can be easily integrated into many existing manufacturing systems to facilitate the mass production of encapsulation thin films. Contrary to traditional vacuum deposition methods, the entire AP-PECVD process is potentially very cost effective, as films can be generated at high throughput without the need for any large footprint vacuum equipment.[9] The in-line processing is hence very versatile and relatively straightforward.

To date, roll-to-roll AP-PECVD has been successfully used to produce ultra-smooth,[25] 100 nm single layer silica-like thin films on a polyethylene 2,6 naphthalate (PEN) substrate that demonstrated a good effective water vapour barrier performance of 1.8×10^{-3} g m^{-2} day^{-1} (at 40 °C, 90% relative humidity (RH)).[11] It was found that an increased substrate temperature

and decreased precursor mass flow,[11] in combination with an enhanced duty cycle or power density,[26] had a profound positive effect on the chemical composition of the silica layers and therefore upon the permeation properties of the films. AP-PECVD has therefore shown particular promise as a technique in the field of protective layer synthesis for flexible solar cells, which have a water vapour transmission rate (WVTR) requirement of 10^{-3} g m^{-2} day^{-1}.[9,27,28] However, this technology is also intended for the production of permeation barriers for flexible organic light emitting diodes (OLEDs), which have a significantly more demanding WVTR requirement of 1×10^{-6} g m^{-2} day^{-1} (at 25 °C, 40% RH),[5,6,10] to ensure the device lifetime of 10000 h is met.[5]

Previous studies have shown that single layer barrier performance is often limited by defects,[2,4,9,11,26,29] as the means by which the films are deposited can make the inorganic layers highly susceptible to cracking or pinhole formation.[9,11,26] And contrary to theoretical assumptions, increasing the thickness of the single layer barriers does little to improve their performance. Thick inorganic layers on polymer substrates have been found to be more prone to cracking and delamination than their thinner counterparts.[30]

To circumvent these issues, organic-inorganic multilayer barriers,[4,6–10,17,18,29] have been reported as a successful substitute to prevent the formation,[1,4,6,9] and propagation of pinholes.[9] Typical WVTR values for these encapsulation barriers are within the region of 10^{-5} g m^{-2} day^{-1} (at 30 °C, 90% RH), therefore almost achieving the OLED protection requirement. They commonly consist of organic polymeric-Al_2O_3 composite layers deposited using techniques such as sputtering, atomic layer deposition (ALD) and molecular layer deposition (MLD) processes.[4,7,8] However, the generation of these encapsulation barriers can be highly expensive, due to the alternate vacuum deposition processes usually required for their synthesis.[9]

The encapsulation potential of hybrid inorganic layered architectures comprising an inorganic dyad, or nano-laminates with different chemical compositions and densities, was recently evaluated.[12,16,31–34] Notable barrier performances were demonstrated, highlighting the synergistic effects of the inorganic layered architecture. The majority of these particular hybrid structured layers were, however, produced both at low pressure and using low deposition rate processes. Conversely, Starostin et al.[16] showed that a combination of roll-to-roll AP-PECVD and stationary plasma assisted ALD could be used to deposit a multilayer silica-alumina moisture permeation barrier on a polymeric substrate that exhibited excellent intrinsic (10^{-5} – 10^{-6} g m^{-2} day^{-1} (at 20 °C, 50% RH)) and good effective (10^{-3} g m^{-2} day^{-1} (at 40 °C, 90% RH)) WVTR performance. The promising result was attributed to two phenomena. First, the enhancement of the polymeric substrate through the use of the mechanically stabilising AP-PECVD silica 'buffer layer'. And second, the 'capping' of the nano-pores in the silica buffer layer by the thin ALD alumina 'barrier layer'.

Therefore the objective of the presented work is to attempt to synthesise high performance bilayer silica-like encapsulation films comprising a thin, dense 'barrier layer' and comparatively thicker, less dense 'buffer layer' using roll-to-roll AP-PECVD. By using the same material in the multilayer film architecture, and by having roll-to-roll AP-PECVD as the only deposition method, renders this investigation highly industrially and commercially relevant to the eventual large scale production of encapsulation barriers for flexible OLEDs. Furthermore, the influence of reactant gas concentrations and the input energy per precursor molecule during the deposition of the barrier layer will be explored. It is likely that these parameters will influence the chemical composition, porosity and hence encapsulating function of the film. The energy consumption per deposited barrier area for single and bilayer films will be evaluated, in addition to the significance of the buffer layer with respect to the encapsulation performance of the overall films.

Experimental Section

Encapsulation film synthesis

A glow-like AP dielectric barrier discharge (DBD) in a roll-to-roll set-up open to ambient air was used to deposit 90 ± 6 nm silica-like bilayer films comprising a 30 ± 4 nm barrier layer and 60 ± 6 nm buffer layer (see **Figure 1**) by PECVD. In addition to the bilayer encapsulation films, 30 ± 5 nm single layer barrier films were synthesised so that the significance of the 60 nm buffer layer with regard to the bilayer encapsulation performance could be evaluated.

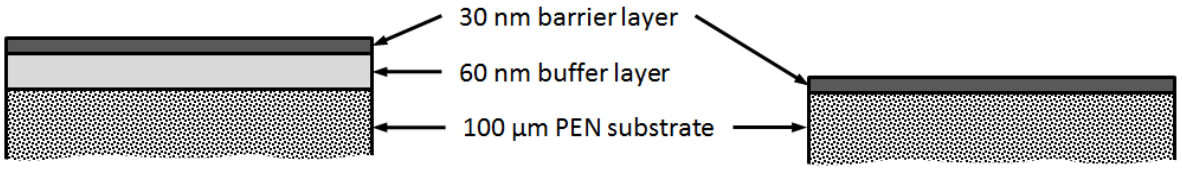

Figure 1. Elementary representation of the silica-like bilayer and single layer films deposited by means of atmospheric pressure-plasma enhanced chemical vapour deposition using a roll-to-roll type dielectric barrier discharge.

A schematic representation of the AP-PECVD reactor is shown in a recent publication by Starostin et al.[11] The DBD was ignited between two cylindrical rotary drum electrodes each with a radius of 120 mm and separated by a 0.5 mm gaseous gap. The electrodes were connected to a matching network, power supply, a voltage probe (Passive High Voltage Probe P6015A, Tektronix) and current probe (Pearson current monitor model 4100, Pearson Electronics, Inc.). The electrodes were heated to 80 ± 1 °C by means of spiral oil-filled tubes located on the inner surface of the metal electrode casing.

Thermally stabilised optical grade polyethylene 2,6 naphthalate (PEN) foil (Teonex Q65FA, Teijin DuPont Films) with a width and thickness of 180 mm and 100 µm respectively, was positioned over each drum electrode, acting as both the dielectric layer in the DBD system

and the substrate upon which the silica layers were deposited (see Figure 1). The PEN polymeric web was connected to independent roll-to-roll foil transport and tension control systems. The foil transport speed was fixed at 400 mm min^{-1} to ensure a 60 nm deposition during the buffer layer synthesis, and varied from 200 – 16 mm min^{-1} for the bilayer barrier synthesis (200 – 32 mm min^{-1} for the single layer barrier) to guarantee a 30 nm deposition. An infrared camera (FLIR A320, FLIR Systems Co Ltd.) was used to monitor the temperature of the substrate during the deposition process.

The plasma was created using a high frequency generator (L3001, Seren Industrial Power Systems), tuned within the range 180 – 200 kHz in order to optimise forward power matching. The PECVD reactor was operated in the pulsed mode, with pulse lengths of 800 μs and a 90% duty cycle. The voltage amplitude measured between the two drum electrodes was 2 – 3 kV. The reflected power was generally in the range 2 – 5% of the forward signal, and the power dissipated in the discharge was 600 W. This corresponded to a specific power density of approximately 0.2 W mm^{-2}, assuming an effective plasma discharge width of 150 mm, and a 20 mm expansion along the gas flow. The peak current density averaged over treated surface area was estimated to reach up to 1.7 mA mm^{-2}. The $I - V$ waveforms of the discharge during deposition can be seen in a publication from Starostin et al.[11] In order to monitor the uniformity of the plasma throughout the deposition process, a sensitive array camera (Eclipse EC-11-05h40, DALSA) with a 13 μs frame integration time was utilised.

The reactant gases in each case were oxygen (technical grade) and tetraethyl orthosilicate ($Si(OC_2H_5)_4$, TEOS) (≥99.0%, Sigma-Aldrich). The precursor gas, TEOS, was injected via a controlled evaporation mixer unit (CEM-Technology, Bronkhorst HIGH-TECH B.V.), where the vapours were combined with 1 slm argon (technical grade). The carrier gas in all cases was nitrogen (technical grade), with a flow of 15 slm for buffer layer syntheses and 20 slm for barrier layer synthesis. All four gases were combined in the gas injector before being

released into the plasma. The reactant gas flows for buffer layers were kept constant at 8.2×10^{-3} slm TEOS and 1.8 slm oxygen. However, in order to vary the input energy per TEOS molecule for the barrier layers and therefore the layer densities, the TEOS and oxygen gas flows were adjusted with a fixed ratio of 4.5×10^{-3} in the range of 1.8×10^{-3} – 0.1×10^{-3} slm and 0.4 – 0.025 slm respectively for the bilayer barriers (and 1.8×10^{-3} – 0.2×10^{-3} slm TEOS; 0.4 – 0.05 slm oxygen for the single layer barriers). This resulted in the deposition of bilayer barriers with input energies ranging from 6 – 80 keV/TEOS molecule (and input energies ranging from 6 – 35 keV/TEOS molecule for single layer barriers). **Equation 1** below,[11] related to the Yasuda composite power parameter,[35] was used to calculate the input energy per TEOS molecule for the barrier layers,

$$Energy\ per\ TEOS\ molecule = \frac{P_d}{R_{dep}\rho} \cdot \frac{M}{N_A} \quad (1)$$

where P_d is the power density in the discharge, R_{dep} is the deposition rate of SiO_2 layers simultaneously upon two substrate webs,[11] (also expressed as $\frac{dh}{dt_{dep}}$, where h and t_{dep} are film thickness and deposition time respectively), ρ is the density of amorphous SiO_2 (2.2 g cm^{-3}), M is the molar mass of SiO_2 and N_A is Avogadro's Number. Contrary to the Yasuda composite power parameter that was originally used to determine input energies for plasma polymerisation,[35] Equation 1 is based not upon the flow rate and molecular weight of the precursor molecule, but upon factors directly related to the deposited amorphous silica layer.[11] For the studied conditions, the reactor was operating in the complete precursor depletion mode.

To investigate the effect of reactant gas concentrations on the resulting properties of the bilayer barriers, a second set of films were produced with the same buffer layer, but barrier

layers with TEOS to oxygen gas flow ratios of 1.5×10^{-3}:1 (TEOS vapour flows ranging from 1.8×10^{-3} – 0.1×10^{-3} slm; oxygen gas flows ranging from 1.2 – 0.075 slm). Despite the increased oxygen flow rate, the input energy per TEOS molecule for these films remained within the range 6 – 80 keV, due to the identical TEOS vapour flows. It should be noted that because of system limitations, for films deposited with barrier layer oxygen gas flows below 0.075 slm, air was used as the reactant gas in place of oxygen.

Spectroscopic ellipsometry (SE) was performed using a variable angle spectroscopic ellipsometer (M-2000D, J.A. Woollam Co. Inc.) in the wavelength range of 400 – 1000 nm in order to determine the thickness of the buffer layers, the combined buffer-barrier bilayers and the single layer barriers post-deposition. The Cauchy dispersion function was used to model the PEN substrate and the silica-like thin films as two separate entities. The optical model did not take into account the substrate anisotropy; however sample orientation was consistent for each measurement.

Compositional and performance analysis

Attenuated total reflectance-Fourier transform infrared (ATR-FTIR) absorption spectroscopy was performed using *un*-polarised light (Frontier FT-IR/FIR Spectrometer, PerkinElmer; Frontier UATR Ge/Ge, PerkinElmer) to investigate the silica-like network structure of the barrier layers, with particular focus upon the Si-OH, SiO-H and HO-H spectral peaks. This set-up utilised a Ge crystal with a 45º face angle and one internal reflection. Spectra were obtained at a fixed angle of 45º, which resulted in a penetration depth range of 165 – 1016 nm for the selected wavenumber range of 4000 – 650 cm^{-1}. To minimise the effect of background noise, 16 scans were acquired for every measurement. The absorbance spectrum of the substrate was subtracted from each sample spectrum and all spectra were interpreted assuming that an increase in peak absorption intensity equated to an increase in the presence

of the corresponding functional group. Deconvolution of all spectral peaks was carried out (Peak Analyzer – Fit Peaks (Pro), OriginPro 9.1) in order to determine the position, full width at half maximum (FWHM) and intensity of each elementary contribution. For the purpose of this analysis, a separate set of samples were investigated as the nature of the original silica-like bilayer films, namely the combination of the extremely thin barrier layers and the dominant PEN FTIR absorption peaks, meant the quality of the subtracted barrier layer silica-like FTIR absorption spectrum was particularly poor. Therefore, a set of ~200 nm equivalent barrier layer-type films that had been deposited onto a polyethylene terephthalate (PET) substrate pre-coated with a 1 μm thick layer of polyvinylidene chloride (PVDC) were analysed instead. The FTIR absorption spectrum of PVDC was neutral enough not to impede the absorption spectrum of the silica-like barrier layers, thereby ensuring 'clean' spectra could be obtained.

In order to determine the stoichiometry of the buffer and barrier layers, X-ray photoelectron spectroscopy (XPS) was performed (AMICUS / ESCA 3400, Kratos Analytical Ltd). The measurement was carried out using a Mg K_α X-ray source with a photon energy of 1254.6 eV, in combination with 25 cycles of 30 second monatomic argon ion beam etching with an ion energy of 0.5 kV. The resulting spectra were processed using CasaXPS software.

Atomic force microscopy (AFM) (Park NX10, Park Systems) was performed to investigate the surface morphology of the PEN substrate, the buffer layer and the bilayer barriers. The measurement was implemented in non-contact mode, using a tip with a radius of approximately 8 nm. Images of 512×512 pixels obtained with a scanning area of 2×2 μm^2, were then processed using Gwyddion software in order to obtain root mean square (RMS) roughness values and cross-sectional height profiles of the layers.[36] The RMS roughness of the pristine PEN substrate was 1.75 ± 0.04 nm.

The effective WVTR of both bilayer samples comprising barrier, buffer and substrate layers, and single layer samples comprising barrier and substrate layers were determined using a Deltaperm (Technolox Ltd.), with set conditions of 40 °C, 90% RH. This measurement therefore took into account the overall permeation of the films; including contributions from macro-defects, and the intrinsic microstructure (nano-defects and gas transport through the amorphous silica-like lattice itself).[37] The Deltaperm is a direct pressure device that fulfils both the ASTM D 1434-82 (2003) standard for permeation measurements and ISO 15106-5:2015, and has a WVTR limit of 2×10^{-4} g m^{-2} day^{-1}. Sample areas of 50 cm^2 were investigated, with each measurement lasting for 100 – 150 hrs in order to ensure the permeation rate had stabilised. The chamber pressure downstream of the sample was recorded each minute, and the WVTR calculated from the output (*x*-variable coefficient and *x*-variable standard error) from a linear regression of the final 200 downstream pressure data points. The WVTR of the pristine PEN substrate was 1.7 g m^{-2} day^{-1}. From the Deltaperm measurements, data concerning the lag-time (the time taken for the WVTR to reach a steady-state) was also obtained for bilayer samples deposited at a reduced oxygen flow rate. The lag-time was calculated from the *x*-axis intercept of an extrapolated line from the steady-state region of the curve, for a plot of downstream pressure expressed as a function of time (see **Figure 2**). The lag-time of the pristine PEN substrate was approximately six hours.

In turn from the lag-time results, the apparent diffusion coefficient D, of the encapsulation layer was calculated for each sample using **Equation 2**,

$$D = \frac{h^2}{6t_{lag}} \tag{2}$$

where h is the thickness of the encapsulation layer and t_{lag} is the lag-time.[38] In this specific case, as the combination of the buffer layer and barrier layer contributed to the overall

apparent diffusion coefficient of the bilayer films, an encapsulation layer thickness h of 90 nm was used, rather than assuming the 30 nm barrier layer was the sole contributing factor.

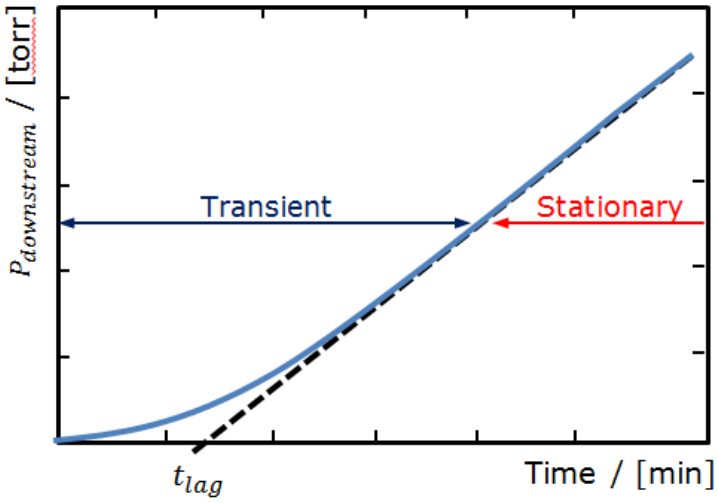

Figure 2. Conceptual plot of cumulative permeation data (downstream pressure vs time), defining lag-time and steady-state regimes for a single-layer system.[38]

Results and Discussion

The ATR-FTIR spectroscopic analysis of the barrier layers is shown in **Figure 3** and **4**. It is understood that the degree of porosity in a silica-like thin film is directly correlated to the presence of hydroxyl groups (-OH) in the network structure.[39–43] The presence of this functional group disrupts the continuous -Si-O-Si-O- network and in turn increases the porosity of the thin film. Figure 3a and 3b show the hydroxyl (O-H) stretching region (4000 – 3000 cm^{-1}) and silanol (Si-OH) stretching region (930 cm^{-1}) respectively. Three individual hydroxyl stretching components are widely acknowledged to combine to form the large peak observed between 4000 and 3000 cm^{-1}. An isolated silanol (*i*SiO-H) stretch is thought to occur at 3650 cm^{-1},[44–46] the hydroxyl stretch of silanol groups (*n*SiO-H) involved in hydrogen bonding (neighbouring silanol groups) is said to appear at 3450 cm^{-1},[45–47] and finally the hydroxyl stretch due to water molecules (HO-H) trapped within the silica network

is understood to arise at 3250 cm^{-1}.[43,45,47] The spectra depicted in Figure 3a were therefore deconvoluted and the specific peak centres, FWHM and absorbance of each individual hydroxyl stretch portrayed in Figure 4 as a function of the input energy per TEOS molecule during the barrier deposition process, together with equivalent data from the spectra in Figure 3b for the Si-OH stretch.

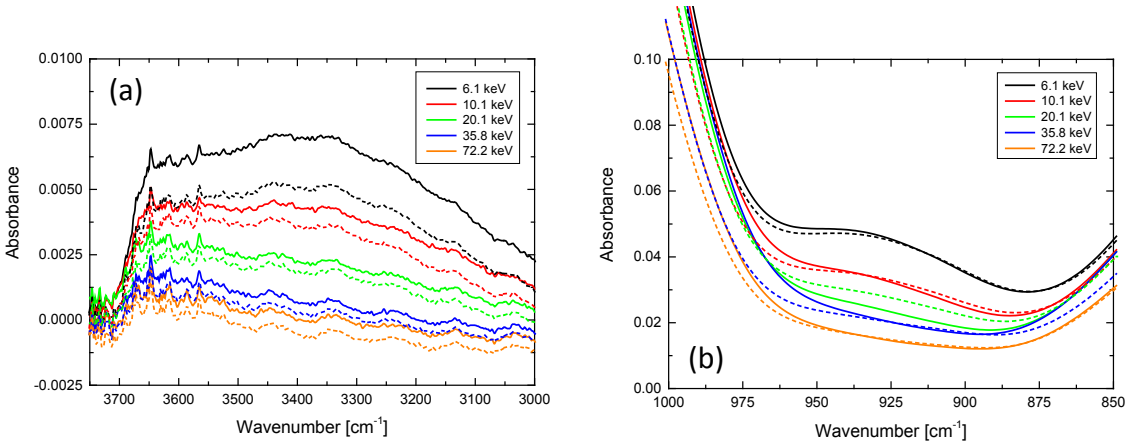

Figure 3. ATR-FTIR absorption spectra showing: (a) the hydroxyl (O-H, 4000 – 3000 cm^{-1}) stretching region and (b) the silanol (Si-OH, 930 cm^{-1}) stretching region of 200 nm silica-like thin films deposited with input E/TEOS from 6.1 – 72.2 keV onto a modified PET substrate using AP-PECVD under conditions replicating those of the barrier layer synthesis: (solid lines) barrier layers deposited at a reduced oxygen flow rate; (dashed lines) barrier layers deposited at an increased oxygen flow rate.

Subtle variations in the specific peak centre are known to indicate fluctuations in the strength and length of bonds present in the assigned functional group, as is outlined in **Equation 3** (Hooke's Law) below,

$$\bar{\nu} = \frac{1}{2\pi c}\sqrt{\frac{k}{\mu}} \qquad (3)$$

where $\bar{\nu}$ is the fundamental vibrational frequency, c is the speed of light, k is the force constant (the proportionality constant relating to the force required to extend a bond) and μ is the reduced mass (**Equation 4**),

$$\mu = \frac{m_1 m_2}{(m_1 + m_2)} \tag{4}$$

where m_1 and m_2 are the component masses for the chemical bond under consideration.[48] Therefore, any increase in the frequency of a peak can potentially be attributed either to an increase in the strength of the chemical bond in question, or a decrease in the reduced mass of the two atoms associated with said chemical bond.

The peak FWHM is acknowledged to be indicative of the degree of variation in bonding arrangements surrounding a particular functional group.[49–52] For instance, interactions such as hydrogen bonding can influence the chemical environment of certain functional groups.

The absorbance, or peak intensity A, as defined in **Equation 5** (the Beer-Lambert Law) below, can provide information relating to the concentration of species present,

$$A = \varepsilon l c \tag{5}$$

where A denotes the measured absorbance, ε is the molar attenuation coefficient (or molar absorptivity), l is the path length of light and c is the concentration of species present. Fundamentally, the equation states that an increase in peak absorbance correlates directly with an increase in concentration of species associated with the alleged peak.

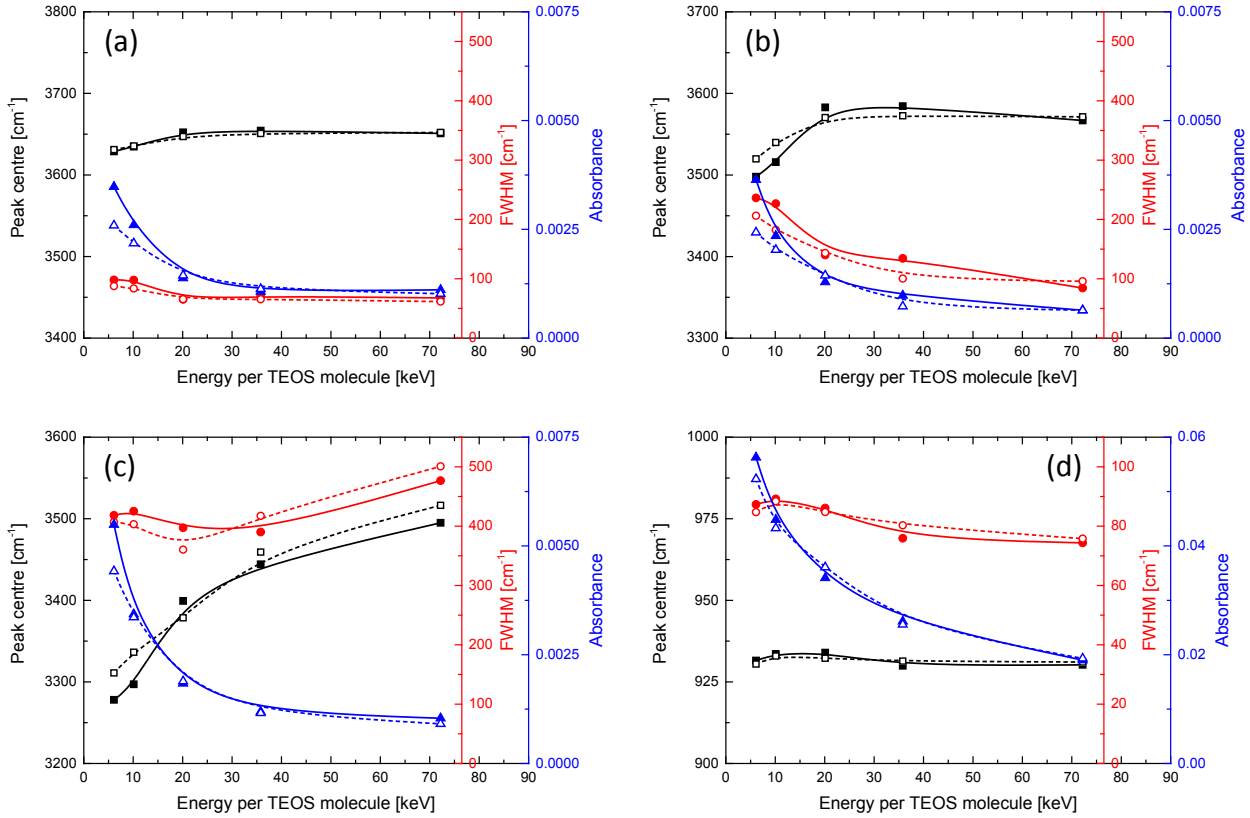

Figure 4. Deconvolution of the ATR-FTIR absorption spectra shown in Figure 3 illustrating the specific peak centre (black; square), FWHM (red; circle) and absorbance (blue; triangle) as a function of increasing input energy per TEOS molecule for the synthesis of the barrier layer for: (a) isolated SiO-H stretch; (b) neighbouring SiO-H stretch; (c) HO-H stretch and (d) Si-OH stretch. (Solid lines) barrier layers deposited at a reduced oxygen flow rate; (dashed lines) barrier layers deposited at an increased oxygen flow rate.

The data in Figure 3 and 4 clearly illustrate that the absorbance of all hydroxyl groups in the barrier layers decrease with increasing input energy per TEOS molecule during the deposition process, to levels where the presence of any hydroxyl group is virtually undetectable. A reduction in the concentration of network disrupting silanol groups, and likewise the concentration of water trapped within the pores, would suggest that the intrinsic microstructure of the silica network gradually increases in density as a function of increasing

deposition input energy. The FWHM of each hydroxyl peak is simultaneously seen to decrease with decreasing film porosity due to a decline in the number of different chemical environments or bonding arrangements. As a consequence of a decreased number of pores, there are less neighbouring silanol groups and less water molecules present for hydrogen bonding interactions to occur. Thus the FWHM of each peak is decreased. Unsurprisingly, this decline in FWHM is therefore most noticeable for the *n*SiO-H stretch. The deviation in the FWHM trend seen for the trapped water (HO-H) stretch is likely to be due to the error involved in the deconvolution of an essentially non-existent peak. Finally, the specific peak centre is observed to increase in wavenumber in all cases with increasing film density, most likely due to an increase in the force constant k, of the O-H and Si-OH bonds, since the reduced mass of the vibrating atoms μ, remains unchanged. This is an outcome of a decrease in the degree of hydrogen bonding interactions in the network, meaning that the strength of the O-H (and Si-OH bonds to some extent) increase, resulting in a slight rise in vibrational frequency. Therefore it is likely that by increasing the input energy per TEOS molecule during the synthesis of the barrier layer, a gradual improvement should be observed with regard to the bilayer and single layer encapsulation barrier performance; a phenomenon that was observed at lower input energies by Starostin et al.[11]

From the ATR-FTIR analysis it is also apparent at these particular deposition input energies, that the oxygen flow rate during the barrier layer deposition has a minimal effect upon the concentration of hydroxyl groups present in the silica-like network structure of the barrier layers. Therefore, it is unlikely that the oxygen flow rate should influence the encapsulation barrier performance of the bilayer films.

Figure 5 shows the O:Si ratios of the barrier and buffer layers obtained from XPS analysis of the bilayer films deposited under different conditions. It is fairly evident that increasing the input energy per TEOS molecule during the deposition process leads to a barrier layer with

an O:Si ratio closer to the desired SiO_2 stoichiometry. The oxygen flow rate during the deposition process, however, appears to have little or no influence at these specific input energies, on the O:Si ratio of the resulting barrier film. Both these findings complement the ATR-FTIR results, signifying that by increasing the input energy per TEOS molecule during the deposition of the barrier layer, a denser and therefore superior encapsulation film should result; while varying the oxygen flow rate appears to have no influence upon the chemical composition of the film and hence a negligible effect should be observed with respect to encapsulation performance.

The percentage elemental composition of the barrier layers is presented in **Table 1**. It is therefore possible that the silica-like barrier layers are not completely pure, with small percentages of carbon and nitrogen also present in the network.

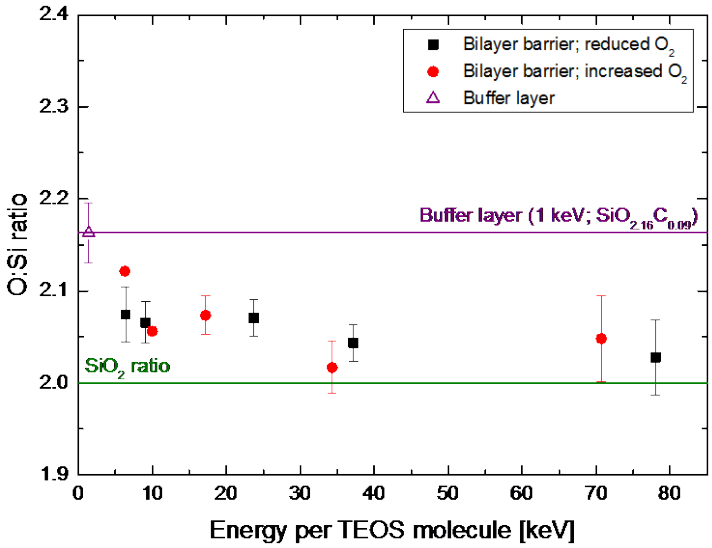

Figure 5. O:Si ratio obtained from XPS analysis with respect to increasing input energy per TEOS molecule for the synthesis of the bilayer barrier during the deposition process.

Table 1. XPS compositional analysis for bilayer barriers deposited at different input energies per TEOS molecule and oxygen flow rates.

Energy per TEOS molecule / keV	Reduced O_2 flow rate during deposition				Increased O_2 flow rate during deposition			
	Si [%]	O [%]	C [%]	N [%]	Si [%]	O [%]	C [%]	N [%]
6	31.3	64.8	3.3	0.6	31.1	66.0	2.1	0.7
10	31.6	65.2	2.9	0.6	31.6	65.0	2.7	0.8
20	31.0	64.2	3.5	1.3	31.1	64.5	3.5	1.0
36	31.8	65.0	2.3	0.9	32.0	64.5	2.4	1.1
72	31.5	64.0	3.2	1.3	31.8	65.2	1.7	1.3

AFM micrographs presented in **Figure 6** illustrate the typical surface morphologies of the bilayer barriers, the buffer and the PEN substrate layers. From these images, it is reasonably clear that the morphology of the buffer and subsequent barrier layers follow that of the PEN substrate; a phenomenon that was also observed by Premkumar et al.[25,53] The buffer layer does however appear to show a greater number of small, high features. This could be the result of incomplete precursor breakdown due to the increased precursor flow rate required for the deposition of this layer and thus reduced plasma residence time. Further investigation is required however, in order to fully verify this.

Topographic analysis displayed in **Figure 7** reveals that the bilayer barriers are extremely smooth, with RMS roughness values for all bilayer films less than 1.5 nm. This RMS roughness value is considerably less than the PEN substrate, which has an RMS roughness of 1.75 ± 0.04 nm. The use of the buffer layer is potentially responsible for the exceptionally smooth bilayer barriers, as it appears to smoothen the PEN substrate profile in preparation for the bilayer barrier deposition. This buffer layer-induced substrate smoothening is also known to be an important factor with regard to reducing the gas permeation rate of the final films.[16,54]

Neither the input energy per precursor molecule, nor the oxygen flow rate during the deposition process appears to have any obvious effect upon the RMS roughness of the bilayer

barriers. This again is likely to be a consequence of the buffer layer in the bilayer architecture. Height profiles of the layers also shown in Figure 7, highlight that the local roughness is potentially also decreased for the bilayer barrier films compared to the PEN substrate, as the variation in height between neighbouring peaks is seen to reduce.

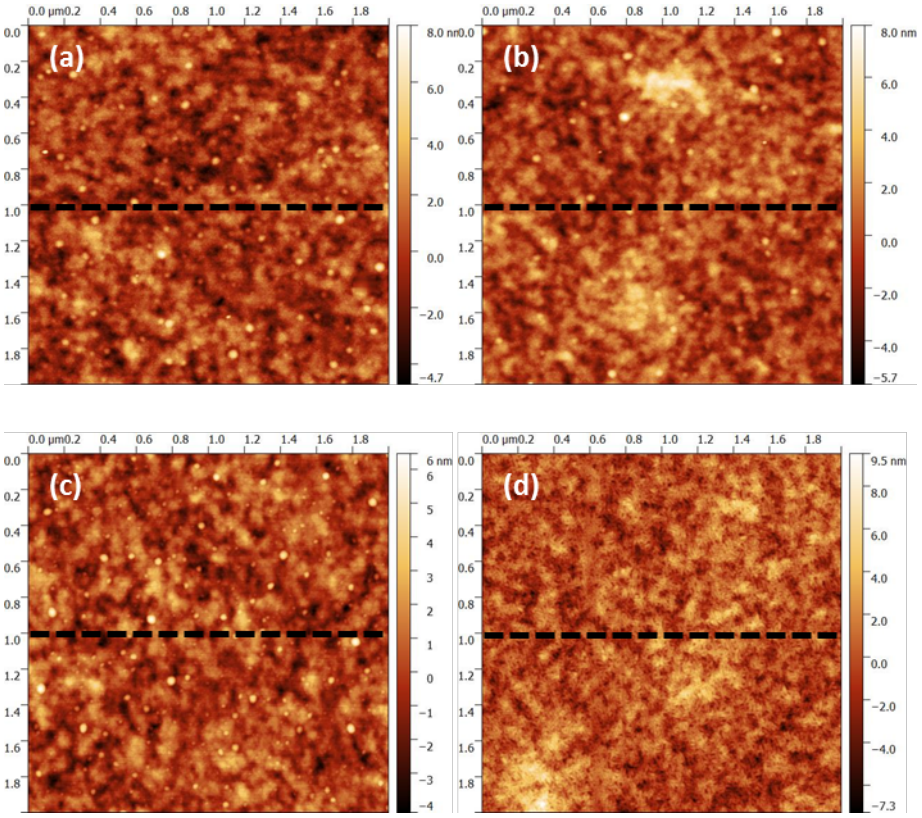

Figure 6. AFM micrographs illustrating the surface morphology of: (a) the bilayer barrier deposited with a reduced oxygen flow rate at 37.2 keV/TEOS molecule; (b) the bilayer barrier deposited with an increased oxygen flow rate at 34.3 keV/TEOS molecule; (c) the buffer layer; (d) the PEN substrate.

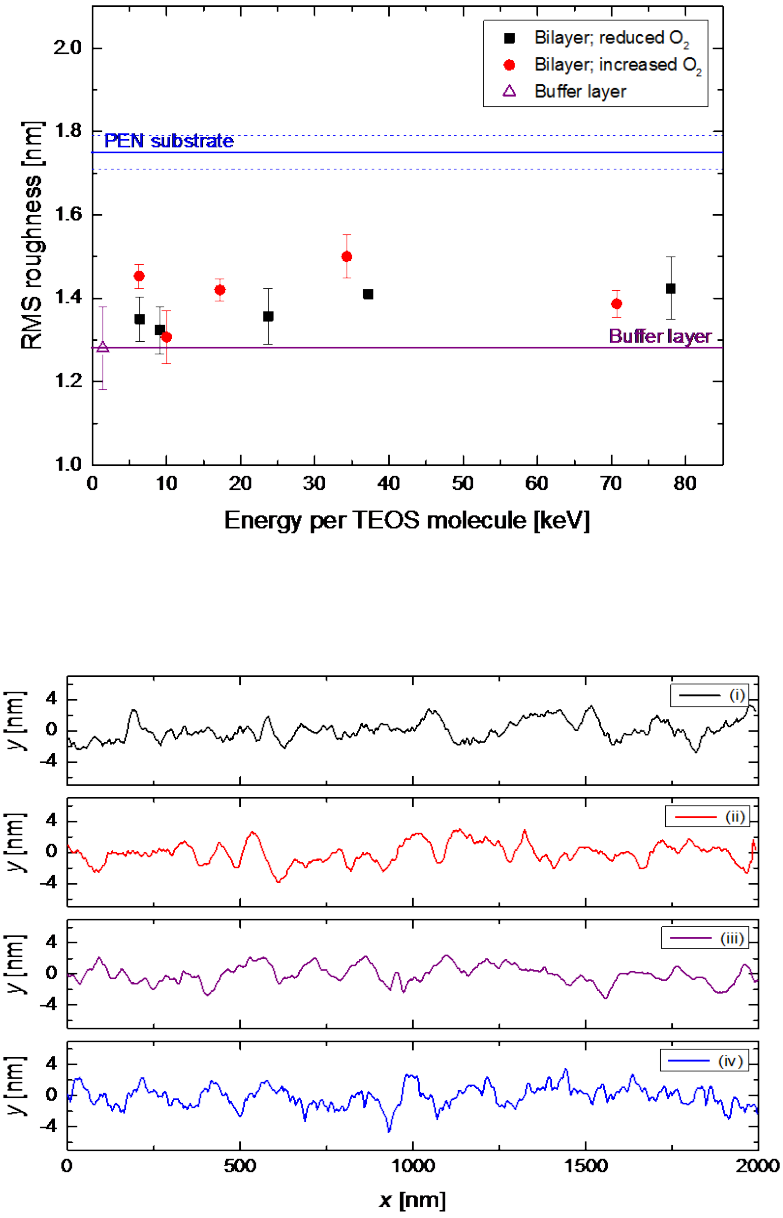

Figure 7. Topographic data obtained from AFM micrographs (Figure 6): (a) RMS roughness plotted as a function of increasing input energy per TEOS molecule for the synthesis of the barrier layers during the deposition process; (b) typical height profiles for: (i) the bilayer barrier deposited with a reduced oxygen flow rate at 37.2 keV/TEOS molecule; (ii) the bilayer barrier deposited with an increased oxygen flow rate at 34.3 keV/TEOS molecule; (iii) the buffer layer; (iv) the PEN substrate.

The effective WVTR values (at 40 °C, 90% RH) with respect to increasing input energy per TEOS molecule during the deposition of the silica-like barrier layer for four different film types are shown below in **Figure 8**. As previously stated, this measurement accounted for permeation through the overall film; including contributions from macro-defects, and the intrinsic microstructure (nano-defects and gas transport through the amorphous silica-like lattice itself).[37] By using the bilayer approach, it is therefore possible to surpass the 100 nm single layer barrier limit,[11] and produce films that exhibit a WVTR as low as 6.9×10^{-4} g m^{-2} day^{-1}. Despite this value not quite being low enough to meet the WVTR requirement for flexible OLEDs,[5,6,10] it is however the lowest WVTR obtained to date for a silica-like film deposited upon a polymer substrate by AP-PECVD.

As can be expected, the thickness of the barrier layer has an impact upon the WVTR for films deposited at 6 keV/TEOS molecule, with the 100 nm barrier exhibiting superior moisture barrier properties.[11] This input energy is still relatively low and therefore the intrinsic microstructure of these barrier layers is comparatively less dense, meaning that the barrier thickness has greater influence upon WVTR performance. Nevertheless, increasing the input energy per TEOS molecule for the barrier layer synthesis by a mere 4 keV/TEOS molecule shows a stark improvement in WVTR performance for the bilayer films, to rates equivalent to that of the best 100 nm barrier.[11] The bilayer architecture therefore has the potential to be significantly more successful than the single layer technique, especially at higher input energies. This assumption is confirmed by the poor performance of the 30 nm single layer films, which not only show an increase in WVTR with increasing input energy per TEOS molecule during the deposition process, but to the extent whereby the reduction in performance is almost three orders of magnitude at the highest comparable input energy. The presence of a buffer layer is therefore vital with regard to achieving the remarkable WVTR performance of the bilayer films, especially at higher input energies. The precise function of

the buffer layer is unknown at present, however it is speculated that the layer could provide a means of mechanical stabilisation to the PEN substrate in preparation for the barrier layer deposition, as highlighted by the AFM topographic analysis and in the recent publication by Starostin et al.[16]

An additional particularly remarkable advantage of the bilayer films over the single layer films is the apparent 50% reduction in energy consumption per barrier area required for their deposition, if films of equivalent encapsulation performance and thickness are compared. This is primarily due to the increased throughput necessary for the synthesis of the 30 nm barrier layer, and is a positive consequence with regard to commercialisation of the encapsulation barrier production process using roll-to-roll AP-PECVD.

Figure 8 also illustrates, however, that the trend observed for the bilayers deviates somewhat from the expected gradual decrease in WVTR with increasing input energy per TEOS molecule, predicted by the ATR-FTIR and XPS results. Values are seen to plateau and increase for samples deposited with input energies greater than 20 keV/TEOS molecule for the barrier layer.

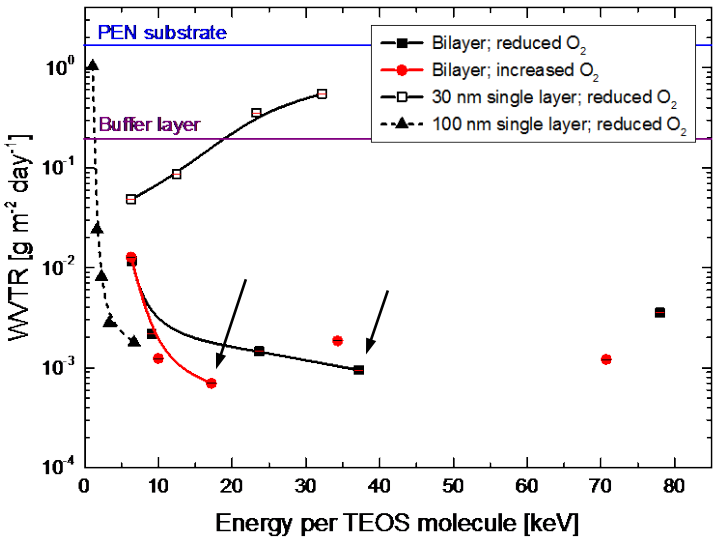

Figure 8. Water vapour transmission rate (at 40 °C, 90% relative humidity) with respect to increasing input energy per TEOS molecule for synthesis of the barrier layer: (black; closed square) values obtained for a 90 nm bilayer film deposited with a reduced O_2 flow rate; (red; closed circle) values obtained for 90 nm bilayer film deposited with an increased O_2 flow rate; (black; open square) a 30 nm single layer barrier deposited with a reduced O_2 flow rate; (black; closed triangle) a 100 nm single layer barrier deposited with a reduced O_2 flow rate.[11]

This deviation can potentially be attributed to the presence of macro-defects in the film, as the intrinsic microstructure of the barrier layers is known from ATR-FTIR and XPS analysis to densify with increasing input energy per TEOS molecule during the deposition. These macro-defects can occur as a result of the harsh processing conditions (sustained plasma and heat exposure) required to achieve very high input energies. Inconsistencies in the quality of the PEN substrate can also potentially contribute to the variations observed. In addition, Figure 8 also shows that increasing the oxygen flow rate during the deposition process can reduce the WVTR for samples with barrier layers deposited from 6 – 20 keV/TEOS molecule. While this may indicate that moisture barrier performance is improved by depositing barrier layers at an increased oxygen flow rate, it is likely that the phenomenon observed is a consequence of varying substrate quality, or gas phase processes resulting in oligomer and particle formation, which thus incorporate into the silica layer causing defects. For the input energies investigated, ATR-FTIR and XPS analysis revealed no obvious indication that the oxygen flow rate had any influence on the density of the intrinsic microstructure of the silica-like barrier layers.

Figure 9 that illustrates the lag-time and apparent diffusion coefficient of the bilayer thin films as a function of input energy per TEOS molecule, complements the WVTR data with

regard to the macro-defect theory. An initial increase in the lag-time, followed by a plateau and notable decrease for films deposited at energies greater than 20 keV/TEOS molecule for the barrier layer can be observed. Since the apparent diffusion coefficient is seen to initially decrease with increasing keV/TEOS molecule, but increase again for films deposited from 25 – 80 keV/TEOS molecule, it is likely that below 20 keV/TEOS molecule, the intrinsic microstructure of the barrier layer dominates the WVTR and lag-time performance, while macro-defects such as pinholes dominate the performance of the barrier layers deposited above 20 keV/TEOS molecule. It is also evident from Figure 9 that the bilayer films with moisture barrier properties governed by their intrinsic silica-like microstructure, exhibit an apparent diffusion coefficient close to that of bulk SiO_2 glass at 40 °C (approximately 9.0×10^{-21} m^2s^{-1}).[38] Had the films deposited at higher energies not been subject to the effect of macro-defects, it is likely that the apparent diffusion coefficient of these films would decrease even further, towards that of bulk SiO_2 glass, as indicated by the ATR-FTIR and XPS findings.

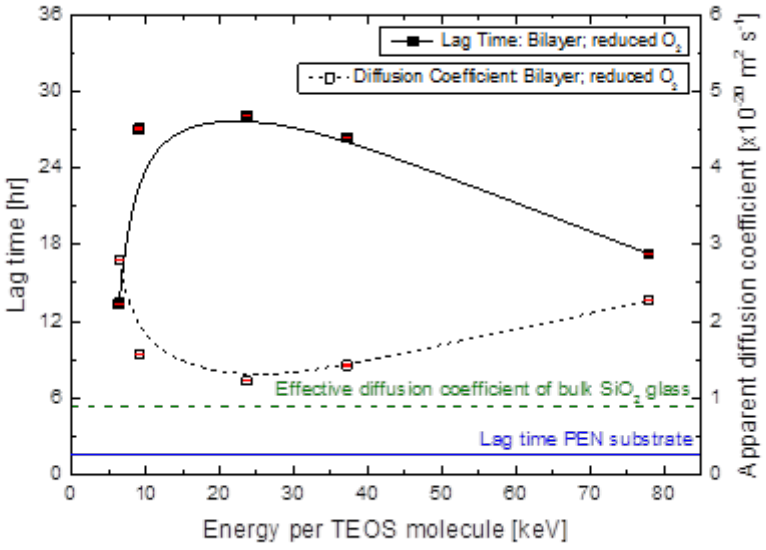

Figure 9. Lag-time (at 40 °C, 90% relative humidity) and corresponding apparent diffusion coefficient with respect to increasing input energy per TEOS molecule for synthesis of the

barrier layer: (black; closed square) lag-time values obtained for a 90 nm bilayer film deposited with a reduced O_2 flow rate; (black; open square) apparent diffusion coefficient values obtained for a 90 nm bilayer film deposited with a reduced O_2 flow rate.

Conclusion

High performance 90 nm silica-like bilayer encapsulation films comprising a 30 nm dense barrier layer and a comparatively less dense 60 nm buffer layer were deposited onto a polyethylene 2,6 naphthalate substrate using a glow-like AP DBD in a roll-to-roll setup by PECVD. TEOS was used as the precursor gas, together with a mixture of nitrogen, oxygen and argon. Effective WVTR measurements confirmed that rates as low as 6.9×10^{-4} g m^{-2} day^{-1} (at 40 °C, 90% RH) were achievable using the bilayer film structure. The presence of a buffer layer within the bilayer architecture, while itself exhibiting a very poor WVTR, was found to critically enhance the encapsulation performance of the 30 nm barrier layers. A remarkable 50% reduction in energy consumption per barrier area required for the deposition of bilayer films compared to single layer silica-like films of equivalent encapsulation performance and thickness was also demonstrated. All bilayer films generated, irrespective of barrier layer deposition conditions, were extremely smooth with RMS roughness values less than 1.5 nm in all cases. This was attributed to possible buffer layer-induced substrate smoothening prior to the bilayer barrier deposition.

It was discovered by complementary lag-time measurements and diffusion coefficient calculations that moisture barrier performance was limited for bilayer films with barrier layers deposited at input energies greater than 20 keV/precursor molecule. Macro-defects in the film possibly resulting from the extreme processing conditions required to achieve the increased input energies per precursor molecule, were proposed as a reason for the limited performance. This was supported by ATR-FTIR and XPS analysis, which showed a gradual

decrease in the silanol content and a steady decline in the O:Si ratio towards 2:1, suggesting that the intrinsic microstructure of the barrier layers actually densified with increasing input energy per precursor molecule and thus intensified processing conditions. The presented findings therefore show that bilayer silica-like encapsulation films deposited under atmospheric conditions have a strong potential for further performance improvement, provided the macro-defect related limitations are addressed.

Acknowledgements: This research received funding from the European Union's Seventh Framework Programme for research, technological development and demonstration under grant agreement number 606889; project ESR7 in the framework of the RAPID (Reactive Atmospheric Plasma processIng – eDucation network) Marie Curie Initial Training Network (www.rapid-itn.eu). The work is also in association with the LIFE12 ENV_NL_000718 'Green plasma process technology for manufacturing of flexible electronics' project. Additional support was given by the FOM Industrial Partnership Programme I31 (APPFF) that is carried out under contract between FUJIFILM Manufacturing Europe B.V. and the Stichting voor Fundamenteel Onderzoek der Materie (FOM), the latter being financially supported by the Nederlandse Organisatie voor Wetenschappelijk Onderzoek (NWO). The author would like to thank Rinie van Beijnen, Emile Gommers and Bruno Korngold (FUJIFILM Manufacturing Europe B.V., Tilburg, The Netherlands) for their technical assistance.

Received: ((will be filled in by the editorial staff)); Revised: ((will be filled in by the editorial staff)); Published online: ((please add journal code and manuscript number, e.g., DOI: 10.1002/ppap.201100001))

Keywords: atmospheric pressure dielectric barrier discharges; bilayer silica-like thin films; encapsulation films; roll-to-roll reactors; water-vapor permeability

[1] J. Lewis, *Mater. Today* **2006**, *9*, 38.

[2] J. -S. Park, H. Chae, H. K. Chung, S. I. Lee, *Semicond. Sci. Technol*. **2011**, *26*, 034001.

[3] N. Grossiord, J. M. Kroon, R. Andriessen, P. W. M. Blom, *Org. Electron*. **2012**, *13*, 432.

[4] Y. C. Han, E. Kim, W. Kim, H. -G. Im, B. -S. Bae, K. C. Choi, *Org. Electron*. **2013**, *14*, 1435.

[5] P. E. Burrows, G. L. Graff, M. E. Gross, P. M. Martin, M. Hall, E. Mast, C. Bonham, W. Bennett, L. Michalski, M. Weaver, J. J. Brown, D. Fogarty, L. S.Sapochak, *Proc. SPIE*. **2001**, *4105*, 75.

[6] M. S. Weaver, L. A. Michalski, K. Rajan, M. A. Rothman, J. A. Silvernail, J. J. Brown, P. E. Burrows, G. L. Graff, M. E. Gross, P. M. Martin, M. Hall, E. Mast, C. Bonham, W. Bennett, M. Zumhoff, *Appl. Phys. Lett*. **2002**, *81*, 2929.

[7] G. L. Graff, R. E. Williford, P. E. Burrows, *J. Appl. Phys*. **2004**, *96*, 1840.

[8] S. -W. Seo, E. Jung, C. Lim, H. Chae, S. M. Cho, *Thin Solid Films*. **2012**, *520*, 6690.

[9] A. Morlier, S. Cros, J. P. Garandet, N. Alberola, *Sol. Energy Mater. Sol. Cells*. **2013**, *115*, 93.

[10] S. Nagai, *Surf. Coatings Technol*. **2015**, *267*, 59.

[11] S. A. Starostin, M. Creatore, J. B. Bouwstra, M. C. M. van de Sanden, H. W. de Vries, *Plasma Process. Polym*. **2015**, *12*, 545.

[12] A. A. Dameron, S. D. Davidson, B. B. Burton, P. F. Carcia, R. S. McLean, S. M. George, *J. Phys. Chem. C*. **2008**, *112*, 4573.

[13] K. Ali, K. -H. Choi, J. Jo, Y. W. Lee, *Mater. Lett*. **2014**, *136*, 90.

[14] L. Hoffmann, D. Theirich, T. Hasselmann, A. Räupke, D. Schlamm, T. Riedl, *J. Vac. Sci. Technol. A Vacuum, Surfaces, Film*. **2016**, *34*, 01A114.

[15] E. Langereis, M. Creatore, S. B. S. Heil, M. C. M. van de Sanden, W. M. M. Kessels, *Appl. Phys. Lett*. **2006**, *89*, 081915.

[16] S. A. Starostin, W. Keuning, J. -P. Schalken, M. Creatore, W. M. M. Kessels, J. B. Bouwstra, M. C. M. van de Sanden, H. W. de Vries, *Plasma Process. Polym*. **2016**, *13*, 311.

[17] S. Majee, B. Geffroy, Y. Bonnassieux, J. -E. Bourée, *Surf. Coatings Technol.* **2014**, *254*, 429.

[18] S. Majee, M. F. Cerqueira, D. Tondelier, B. Geffroy, Y. Bonnassieux, P. Alpuim, J. -E. Bourée, *Prog. Org. Coatings*. **2015**, *80*, 27.

[19] P. Alpuim, S. Majee, M. F. Cerqueira, D. Tondelier, B. Geffroy, Y. Bonnassieux, J. -E. Bourée, *Thin Solid Films*. **2015**, *595*, 258.

[20] T. N. Chen, D. S. Wuu, C. C. Wu, C. C. Chiang, H. B. Lin, Y. P. Chen, R. H. Horng, *Thin Solid Films*. **2006**, *514*, 188.

[21] S. Majee, M. F. Cerqueira, D. Tondelier, B. Geffroy, Y. Bonnassieux, P. Alpuim, J. -E. Bourée, *Surf. Coatings Technol*. **2013**, *235*, 361.

[22] S. Zhang, W. Xue, Z. Yu, *Thin Solid Films*. **2015**, *580*, 101.

[23] S. Majee, M. F. Cerqueira, D. Tondelier, J. C. Vanel, B. Geffroy, Y. Bonnassieux, P. Alpuim, J. -E. Bourée, *Thin Solid Films*. **2015**, *575*, 72.

[24] F. J. H. van Assche, S. Unnikrishnan, J. J. Michels, A. M. B. van Mol, P. van de Weijer, M. C. M. van de Sanden, M. Creatore, *Thin Solid Films*. **2014**, *558*, 54.

[25] P. A. Premkumar, S. A. Starostin, M. Creatore, H. de Vries, R. M. J. Paffen, P. M. Koenraad, M. C. M van de Sanden, *Plasma Process. Polym*, **2010**, *7*, 635.

[26] G. Aresta, P. A. Premkumar, S. A. Starostin, H. de Vries, M. C. M. van de Sanden, M. Creatore, *Plasma Process. Polym*. **2010**, *7*, 766.

[27] C. Vallee, A. Goullet, A. Granier, A. van der Lee, J. Durand, C. Marliere, *J. Non-Cryst. Solids*. **2000**, *272*, 163.

[28] N. Kim, W. J. Potscavage, A. Sundaramoothi, C. Henderson, B. Kippelen, S. Graham, *Sol. Energy Mater. Sol. Cells*. **2012**, *101*, 140.

[29] A. S. da Silva Sobrinho, G. Czeremuszkin, M. Latrèche, M. R. Wertheimer, *J. Vac. Sci. Technol. A Vacuum, Surfaces, Film*. **2000**, *18*, 149.

[30] Y. Leterrier, *Prog. Mater. Sci*. **2003**, *48*, 1.

[31] N. Kim, W. J. Potscavage Jr, B. Domercq, B. Kippelen, S. Graham, *Appl. Phys. Lett*. **2009**, *94*, 163308.

[32] P. F. Carcia, R. S. McLean, M. D. Groner, A. A. Dameron, S. M. George, *J. Appl. Phys*. **2009**, *106*, 023533.

[33] A. Bulusu, H. Kim, D. Samet, S. Graham Jr, *J. Phys. D. Appl. Phys*. **2013**, *46*, 084014.

[34] L. H. Kim, K. Kim, S. Park, Y. J. Jeong, H. Kim, D. S. Chung, S. H. Kim, C. E. Park, *Appl. Mater. Interfaces*. **2014**, *6*, 6731.

[35] H. K. Yasuda, *Plasma Polymerization*, Academic Press Inc, Orlando **1985**.

[36] D. Necas, P. Klapetek, *Cent. Eur. J. Phys*. **2012**, *10*, 181. www.gwyddion.net.

[37] A. P. Roberts, B. M. Henry, A. P. Sutton, C. R. M. Grovenor, G. A. D. Briggs, T.

Miyamoto, M. Kano, Y. Tsukahara, M. Yanaka, *J. Memb. Sci*. **2002**, *208*, 75.

[38] S. Nagai, *J. Appl. Phys*. **2013**, *114*, 174302.

[39] W.A. Pliskin, *J. Vac. Sci. Technol*. **1977**, *14*, 1064.

[40] J. Schafer, R. Foest, A. Quade, A. Ohl, K. -D. Weltmann, *Plasma Process. Polym*. **2009**, *6*, S519.

[41] A. Brunet-Bruneau, J. Rivory, B. Rafin, J. Y. Robic, P. Chaton, *J. Appl. Phys*. **1997**, *82*, 1330.

[42] S. C. Deshmukh, E. S. Aydil, *Appl. Phys. Lett*. **1994**, *65*, 3185.

[43] P. Innocenzi, *J. Non-Crystallin. Solids*. **2003**, *316*, 309.

[44] J. A. Theil, D. V Tsu, M. W. Watkins, S. S. Kim, G. Lucovsky, *J. Vac. Sci. Technol. A*. **1990**, *8*, 1374.

[45] M. Creatore, S. M. Rieter, Y. Barrell, M. C. M. van de Sanden, R. Vernhes, L. Martinu, *Thin Solid Films*. **2008**, *516*, 8547.

[46] M. Creatore, J. -C. Cigal, G. M. W. Kroesen, M. C. M. van de Sanden, *Thin Solid Films*. **2005**, *484*, 104.

[47] L. B. Capeletti, I. M. Baibich, I. S. Butler, J. H. Z. dos Santos, *Spectrochim. Acta Part A*. **2014**, *133*, 619.

[48] J. Coates, *Interpretation of Infrared Spectra, A Practical Approach*, in *Encyclopedia of Analytical Chemistry*, (Ed: R. A. Meyers), John Wiley & Sons Ltd, Chichester **2000**, pp. 10815–10837.

[49] M. Nakamura, Y. Mochizuki, K. Usami, Y. Itoh, T. Nozaki, *J. Electrochem. Soc*. **1985**, *132*, 482.

[50] E. Hensel, K. Wollschlager, D. Schulze, U. Kreissig, W. Skorupa, J. Finster, *Surf.*

Interf. Anal. **1985**, *7*, 207.

[51] I. W. Boyd, J. I. B. Wilson, *Appl. Phys. Lett*. **1987**, *50*, 320.

[52] P. G. Pai, S. S. Chao, Y. Takagi, G. Lucovsky, *J. Vac. Sci. Technol. A*. **1986**, *4*, 689.

[53] P. A. Premkumar, S. A. Starostin, H. de Vries, M. Creatore, P. M. Koenraad, W. A. MacDonald, M. C. M. van de Sanden, *Plasma Process. Polym*. **2012**, *9*, 1194.

[54] A. M. Coclite, K. K. Gleason, *J. Appl. Phys*. **2012**, *111*, 073516.

Graphical Abstract

Flexible bilayer silica-like thin films deposited using roll-to-roll AP-PECVD onto a polymeric substrate are presented as a remarkable alternative to single layer encapsulation films. They demonstrate both a notable effective water vapour transmission rate of 6.9×10^{-4} g m^{-2} day^{-1} (at 40 °C, 90% relative humidity) and a 50% reduction in deposition energy consumption per barrier area.

Fiona M. Elam,* Sergey A. Starostin, Anna S. Meshkova, Bernadette C. A. M. van der Velden-Schuermans, Jan B. Bouwstra, Mauritius C. M. van de Sanden, Hindrik W. de Vries.

Atmospheric pressure roll-to-roll plasma enhanced CVD of high quality silica-like bilayer encapsulation films